Coherence studies of pulsed electron beams from point sources

Contact *w.a.bryan@swansea.ac.uk*

A. R. Bainbridge, D. Thorne, W. A. Bryan.
Department of Physics, College of Science, Swansea University, Singleton Park, Swansea, SA2 8PP.

P. Lane, M. Robinson, S. Young, D. Wann.
Department of Chemistry, University of Edinburgh West Mains Road, Edinburgh, EH9 3JJ

R. Chapman, P. Rice, E. Springate.
Central Laser Facility, STFC Rutherford Appleton Laboratory Harwell Oxford, Didcot, Oxfordshire, 0X11 0QX

Introduction

Generation of electron beams is a common activity employed in a wide variety of scenarios in laboratories around the world for a number of purposes. Many of these applications involve applying the electron beam to a target in order to determine a property such as the size or structure of the object; commonly used examples include transmission electron microscopy[1] & scanning electron microscopy, electron diffraction and electron holography[2]. These applications have a common feature in the use of a continuous beam, which can provide high spatial resolution, but removes the ability to perform time-resolved measurements below the nanosecond timescale, such systems being limited by capacitive switching.

Presently, significant progress is being made in developing time resolved measurements using a pulsed electron beam, particularly in the field of electron diffraction studies[3], introducing the use of pulsed electron beams as a complimentary technique to x-ray diffraction studies performed at synchrotron or X-FEL facilities. This is generally referred to as Ultrafast Electron Diffraction (UED). Such a beam can be created by the interaction of an ultrafast laser pulse with a photocathode to generate a short bunch of electrons, followed by either acceleration to relativistic velocities (requiring large voltages and a long beamline) or some compression technique to counter the effects of space-charge repulsion. The current state of the art allows for electron pulses that can be compressed to 100 femtoseconds by means of an RF cavity[4]. This allows electron diffraction to gain time resolution on the timescale of molecular motion, potentially allowing observation of features such as bond formation and charge migration.

Diffraction studies require that the electron beam have a high degree of spatial coherence, quantified by the transverse coherence length, which defines the maximum size of the beam target. An electron beam with a small coherence length cannot form fringes of sufficient contrast to obtain a high resolution image under Fourier transform, nor will the fringes be generated over the whole of the target, dramatically limiting the field of view. For this reason, it is vital that the coherence length of the electron beam be known, and that steps are taken to ensure that it is as large as possible.

Electron coherence of a pulsed beam depends primarily on three parameters: The coherence of the light used to generate the electrons, the temperature at the electron source, and the geometry (the key factor of which is the emission volume) of the photocathode. The requirement for low temperature is difficult to quantify; it is already partially satisfied by having the photocathode in a vacuum chamber, however could be improved by active cooling. There is no simple solution, as cooling may cause residual gas in the vacuum chamber to condense onto the cathode, dramatically reducing its effectiveness. Recent studies have revealed the possibility of using a cooled gas phase source[5].

The final condition can be met by using a shaped cathode in place of traditional flat sheet or film. We are currently investigating the use of a Nanoscale Metal Tip (NSMT), a small piece of wire which tapers to a very sharp point, with a radius of curvature at the tip typically of order 10's of nm. Such a tip is produced by electrochemical etching from gold or tungsten wire. With further refinement such as annealing or electron bombardment it is possible to bring these tips to a single atom end[6], making them a true point source, although the term could reasonably be applied to any tip below 100 nanometers if the electron beam flight path is on a scale of centimeters or meters. The emission occurs from the curved surface at the end of the tip, leading to an emission volume much smaller than the laser focal spot. This is predicted to create highly coherent electrons in comparison to those emitted from a plane cathode, where the emission generally originates from a spot several microns across defined by the tightness of the laser focus. The shape of the tip also concentrates and enhances the electric field, allowing the use of an 800 nm Ti:Sapphire laser oscillator in place of a UV laser[7,8], which may require a more complex and expensive regenerative amplifier and OPA system to produce the required pulse length.

Electron Holography

Measurement of coherence can be performed by means of holography[9], where a wavefront is forced into overlapping with another wavefront from the same source. If there is coherence, an interference pattern will occur, the properties of which allow the transverse coherence length to be measured. An electron beam can be made to interfere with itself by splitting and recombining using a biprism, a positively charged wire between two grounded electrodes that cause the electron beam to split each side of the wire; the positive charge then causes the resulting beams bend towards each other and overlap.

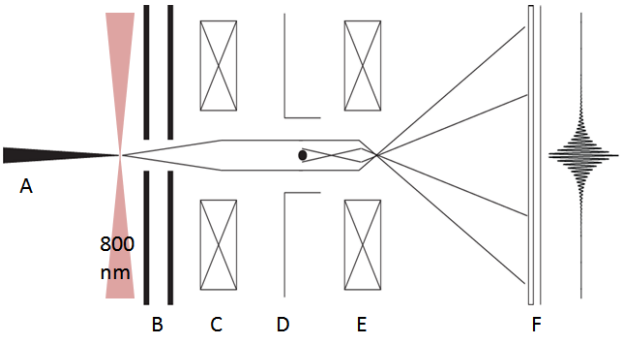

Figure 1: Illustration of the principle of electron holography. Electrons are generated from a source (A) before being accelerated via electrodes (B). The beam is collimated with a magnetic lens (C) before being split by the biprism (D). A second magnetic lens (E) provides high magnification before the beam and resulting interference pattern arrives at the detector (F).

This technique, the principal of which is outlined in figure 1, is traditionally used to determine the structure of an object that has been placed in one of resulting beams. The perturbation of the interference pattern caused by this can be transformed to yield a hologram of said object. Crucially, this is not limited to solid matter, as any electric or magnetic fields around the object will also cause a perturbation, allowing the holography technique to be used to examine local field effects or enhancements.

Apparatus design and construction

An illustration of our equipment is shown in figure 2. The electrons are first generated from the NSMT by either field emission (for a continuous beam) or by interaction with an intense <100 fs 800 nm laser pulse. The tip is held at a high negative bias to define the energy of the resulting beam. The first electrode after the tip is also held at a high negative bias, although slightly lower than the tip. This is adjustable; the bias can be increased to induce field emission or can be reduced to simply provide a steering and accelerating force to ensure that electrons from the tip form a directed beam. The second electrode is held at or near ground, accelerating the beam to its final energy.

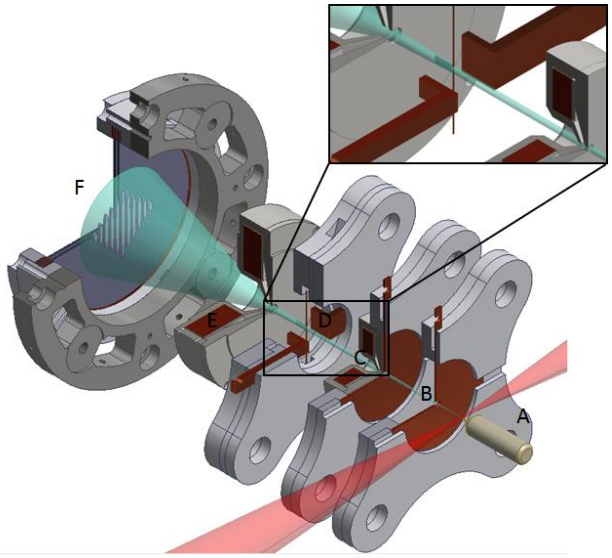

Figure 2: Simplified model of the equipment being used to conduct this experiment. A NSMT in an insulating holder (A) is excited by an 800 nm laser pulse. The resulting electron beam is accelerated by electrodes (B) before being collimated by a lens (C). The beam is then split by the biprism (D and insert), before being magnified by the second lens (E). An MCP, phosphor screen and CCD assembly (F) then records the interference pattern.

Having passed through the second electrode an adjustable magnetic lens is used to collimate the beam, or can even be used to focus onto the biprism to ensure fringe production. The biprism itself consists of a 4 micron diameter tungsten wire, to which a small positive bias can be applied, which defines the crossing angle and position. A grounded L –shaped plate is positioned either side of the wire to complete the biprism. A second magnetic lens is used to pass the beam through a short focus to make it diverge (providing adjustable zoom) before reaching the detector, consisting of an MCP and phosphor screen. A CCD camera then records the resulting interference pattern as a numerical array for analysis by LabView software.

Current results

This is work currently in progress and as such has not yielded measurements of the coherence length at the time of writing. Much progress has been made, however, and the present apparatus is capable of producing and maintaining a stable pulsed electron beam aligned centrally onto the biprism wire. This can be verified by applying a voltage to the wire; a negative bias will split the electron beam in half and cause the resulting beams to diverge, making the position of the wire easily visible. A positive voltage will cross the resulting beams.

Both of these scenarios are displayed in figure 2 for a variety of bias voltages, demonstrating the effectiveness of such a wire. These images of the beam are not magnified to best display the effect, so no fringing is visible.

The current results follow from work as outlined in the previous annual report[10], where it was established that NSMT's of both gold and tungsten can be made to emit stably under focused (and even unfocused for high energy) 800 nm 100fs laser pulses. Basic measurements of the electron energy spectrum have also been reported, highlighting the effect of various laser parameters on the emission characteristics. These measurements are pending refinement, as outlined below.

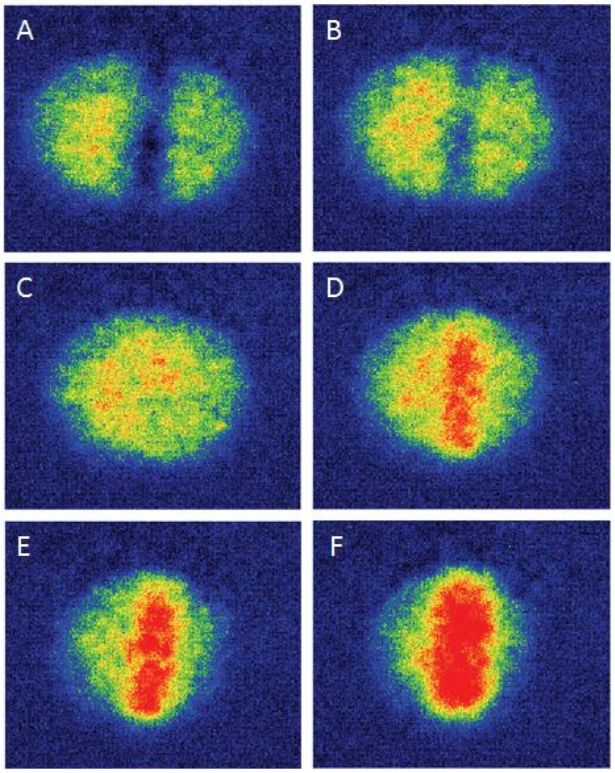

Figure 3: Image of electron beam for a variety of biprism wire voltages: A= - 60 V, B= -30 V, C= 0 V, D= +30 V, E= +60 V and F= +90 V. The negative voltages clearly allow the position of the wire to be seen, and the positive voltages clearly show the resulting split beams being overlapped.

Pending improvements and ongoing experiments

Presently the design of the biprism assembly is being improved to allow for the high magnifications needed to observe fringes that appear on the nanometer scale. A new magnetic lens is currently under construction that replaces the existing simple coil with a lens encapsulated by field-focusing tapered pole pieces. This allows the magnetic field to be concentrated at the beam position, resulting in a comparatively much stronger on-axis field even at low currents. The resulting increase in field strength should allow a short focal length (and by extension higher magnification) even at high beam energies. It is anticipated that this new lens design, illustrated in figure 4, will allow definitive measurements of the transverse coherence length of the electron beam. To the Author's knowledge, this will be the first time this quantity has been measured for a laser induced, pulsed beam from a point source.

In addition, a detailed analysis of the energy spectrum of the emitted electrons is currently underway. Although the width of the spectrum has been determined by previous experiments to be small in comparison to the beam energy, the effect of the energy spread to the temporal dispersion of the electron pulse

(already significant due to Coulomb repulsion) is non-negligible, especially if the electron pulse is due to be compressed by means of an RF cavity or ponderomotive compression. This is being done by means of a Velocity Map Imaging (VMI) spectrometer, which allows both the electron energy spectrum and direction of emission to be simultaneously measured as a function of a variety of parameters such a laser pulse length, intensity and polarization.

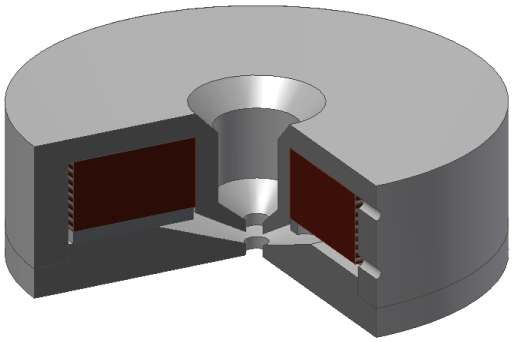

Figure 4: Illustration of the new magnetic lens design featuring field-focusing tapered pole-pieces.

Applications

This work is primarily being done with a view to utilizing the fully characterized pulsed electron beam for UED purposes, examining changing structural dynamics in a variety of systems. Examples include observing the effect of optical pumping on foils or large molecules in the gas state. The most intriguing application, however, is the potential to examine large molecules such as proteins or DNA during their response to an external stimulus, an ability which fully utilizes the high coherence length of the beam. It may also be possible to examine molecules in the solution phase, contained in micron scale droplets. This allows the molecules to be examined in a scenario which much more closely resembles the biological system in which they normally reside, rather than the traditional technique of crystallizing them onto a surface, altering their structure before the measurements can be performed.

In order to achieve this goal, the electron pulses are required to be a few femtoseconds long as they arrive at the target, requiring the addition of a compression stage to the beamline to counteract the temporal dispersion of the pulse. An alternative to the aforementioned RF compression is the use of a shaped laser pulse to apply a spatially modulated potential to the electron pulse in flight. This technique has to date only been treated theoretically, it is the intention of the authors to make an attempt at experimentally verifying the possibility of using this procedure in the very near future.

Conclusions

Work is ongoing to measure the transverse coherence length of pulsed electron beams originating from a laser driven point source. It is anticipated that such beams will be useful in resolving molecular dynamics on a sufficiently short timescale to observe features such as charge migration, bond formation and vibrational motion.

Acknowledgements

Our thanks go to team and support staff at the Artemis laser facility, STFC Rutherford Appleton Laboratory for allowing the use of their facility and producing custom equipment, and to the EPSRC Laser Loan Pool for the loan of the UFL2 laser system.

References

1. Thomas & Midgley, Chem. Phys. 385 (2011) 1-10
2. Hasselbach, Rep. Prog. Phys. 73 (2010) 016101
3. Sciaini & Miller, Rep. Prog. Phys. 74 (2011) 096101
4. Luiten *et al*, Phys. Rev. lett. 105 (2010) 264801
5. Scholten *et al*, Nat. Phys. 7 (2011) 785-788
6. Wolkow *et al*, J. Chem. Phys 124 (2006) 204716
7. Hommelhoff *et al*, J. Phys. B: At. Mol. Opt. Phys. 45 (2012) 074006
8. Batelaan *et al*, New. J. Phys. 9 (2007) 142
9. Wolkow *et al*, New. J. Phys. 15 (2013) 073038
10. Bryan *et al*, CLF Annual Report 2011-2012, 46

Ultrafast spectroscopy of plasmonic nanoantennas using the Pharos/Orpheus laser

Contact *O.Muskens@soton.ac.uk*

Martina Abb
Physics & Astronomy, Faculty of Physical Science and Engineering
Highfield, SO17 1BJ, Southampton

Yudong Wang
Electronics & Computer Science, Faculty of Physical Science and Engineering
Highfield, SO17 1BJ, Southampton

Kees de Groot
Electronics & Computer Science, Faculty of Physical Science and Engineering
Highfield, SO17 1BJ, Southampton

Otto L. Muskens
Physics & Astronomy, Faculty of Physical Science and Engineering
Highfield, SO17 1BJ, Southampton

Introduction

Nanophotonic devices that can efficiently concentrate optical radiation into a nanometer-sized volume are of great interest for many applications in integrated and nonlinear photonics, radiative decay engineering, and quantum information processing. Analogous to their radiowave counterparts, plasmonic nanoantennas are designed to provide a high local field enhancement with efficient coupling to far field radiation in the visible and infrared spectral window. Active control of the resonance spectrum of a plasmonic nanoantenna is a crucial step toward achieving transistor-type nanodevices for manipulation of the flow and emission of light.

We aim to develop a new class of all-optical switches using optical nanoantennas. The antenna switch as proposed by us operates on the transition from the capacitive to conductive coupling regimes between two closely spaced metal nanorods.

Apart from using the optical nonlinearity of the gold itself to provide a switching functionality, it is of interest to interface the plasmonic system to other types of materials which can be tuned using optical, electrical, or magnetic means. In this project, we were interested to explore the ultrafast nonlinear response of antennas on different types of substrates including semiconductors and metal oxides.

In our recent work we have demonstrated a new nanoscale plasmon-induced energy transfer mechanism by fast electron injection from the antenna into the surrounding semiconductor for controlling the optical modes of a nanoantenna-ITO hybrid [1]. The mechanism relies on the mutual interaction of the nanoantenna, which acts as a source for sensitizing the ITO response, and the large free-carrier nonlinearity of ITO, which in return modifies the plasmon resonance. The aim of the current project was to extend measurements to the subpicosecond time domain.

Results

The femtosecond nonlinear optical response of plasmonic nanoantennas was investigated using a regenerative amplified laser system (Pharos/Orpheus). In order to operate this system in a pump-probe configuration, we had to combine the following ingredients: access to (depleted) fundamental and second harmonic outputs of the laser; access to the outputs (signal, idler) of the optical parametric amplifier, and computer control of the OPA wavelength using the Labview software environment.

After some initial problems, the wavelength control was successfully implemented in the second month of the laser loan. We could perform computer controlled scans of the idler over a range 1100-1700nm. We used a chopper and lock-in amplifier to recover the optical intensity, which was detected by an InGaAs photodiode. It was found that the fast transients caused by the individual laser pulses in the 50 kHz repetition rate system resulted in overloads of the lock-in amplifier input. To solve this issue, a low-noise preamplifier (Stanford Research Instruments) with tunable input and output bandpass filters was used to suppress these high-frequency components. Using this configuration, it was possible to perform optical pump-probe experiments at 1 kHz modulation frequency at a signal to noise ratio of around 10^{-4} $Hz^{-1/2}$.

A second challenge consisted of finding the timings of the different outputs. In particular, separate outputs of the depleted pump and the second harmonic were available but since the former was split off before the OPA stage, a significant time difference had to be compensated outside the laser system. However, it was eventually possible to simultaneously access the three outputs (fundamental, SHG, idler) for advanced pump-probe experiments.

Arrays of nanoantennas were fabricated using e-beam lithography. The antennas consisted of two closely spaced gold nanorods as illustrated by the electron microscopy image in Fig. 1. The rods are capacitively coupled in the nanogap, which results in a strong local field enhancement which may be used for nonlinear spectroscopy and sensing.

These types of nanoantennas show a strong plasmonic response in the near-infrared. A transmission spectrum of the nanoantenna arrays obtained using the idler of the Orpheus OPA is shown in Figure 2. The dip at around 1250nm wavelength corresponds to the fundamental longitudinal antenna mode. This mode is associated with a $\lambda/2$ standing wave resonance, where λ is the wavelength of the plasmon polariton (λ is smaller than the vacuum wavelength because of the real part of the permittivity of gold).

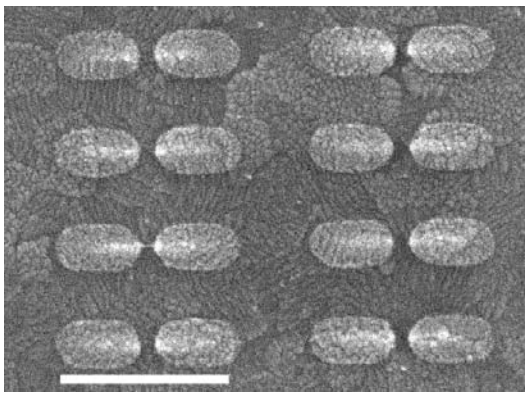

Figure1 Scanning electron microscopy image of nanoantenna array consisting of gold nanorods (scale bar 500nm).

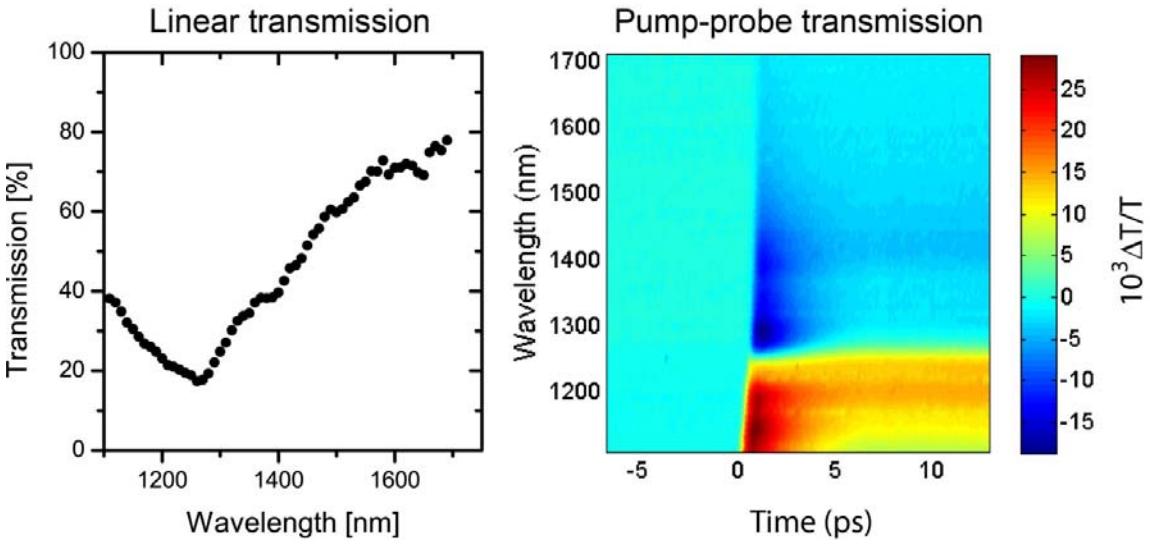

Figure 2 Transmission spectrum (left) and ultrafast pump-probe map of antenna array obtained using Pharos/Orpheus laser system using 515nm pump and OPA (idler) probe.

Simultaneously, we performed ultrafast pump-probe spectroscopy using the output from the amplifier at 1030nm – or its second harmonic at 515nm – as an excitation source. A resulting map of the ultrafast dynamics of the antenna array is shown in the right figure. A fast initial response is observed resulting from the excitation of hot electrons in the gold nanoantenna. The signal is consistent with a combination of transient bleaching and a redshift of the plasmon resonance. The decay agrees with other broadband response reported in literature and follows the two-temperature model of hot electron relaxation in metals [2,3].

Conclusions

The laser loan has enabled us to obtain a variety of results on the ultrafast response of nanoantennas on various active substrates. We are currently preparing publications using this data. Using the information extracted from this study, we are able to target specific materials which may be of interest for interfacing with plasmonics for applications in nonlinear control and ultrafast switching. The realization of an antenna switch is a first step toward a longer-term programme of integration of active plasmonics in various fields of nanoscience, such as ultrafast lasers and quantum optics. The application perspective of the proposed devices is high; antenna switches hold the potential for active control of nanoscale light-matter interaction on ultrafast timescales. This includes, next to transmission and reflection of light, also the radiative decay of emitters, as well as the coupling strength of coherent states of light and matter.

Acknowledgements

The authors acknowledge support from EPSRC through grant EP/J011797/1.

References

1. M. Abb, Y. Wang, P. Albella, C. H. de Groot, J. Aizpurua, and O. L. Muskens, Interference, Coupling, and Nonlinear Control of High-Order Modes in Single Asymmetric Nanoantennas, ACS Nano 6 (7), 6462-6470 (2012).
2. M. Kiel, H. Mohwald, M. Bargheer, Broadband easurements of the transient optical complex dielectric function of a nanoparticle/polymer composite upon ultrafast excitation, Phys. Rev. B 84, 165121 (2011).
3. H. Baida, D. Mongin, D. Christofilos, G. Bachelier, A. Crut, P. Maioli, N. Del Fatti, F. Vallée, Ultrafast Nonlinear Optical Response of a Single Gold Nanorod near Its Surface Plasmon Resonance, Phys. Rev. Lett. 107, 057402 (2011).

Manipulation of a continuous beam of molecules by light pulses

Paul Venn and Hendrik Ulbricht*
Physics and Astronomy, University of Southampton, Highfield, Southampton, SO17 1BJ, UK
(Dated: July 1, 2013)

We experimentally observe the action of multiple light pulses on the transverse motion of a continuous beam of fullerenes. The light potential is generated by non-resonant ultra-short laser pulses in perpendicular spatial overlap with the molecule beam. We observe a small but clear enhancement of the number of molecules in the center fraction of the molecular beam. Relatively low light intensity and short laser pulse duration prevent the molecule from fragmentation and ionization. Experimental results are confirmed by Monte Carlo trajectory simulations.

It is known from both theory [1] and experiment [2–5] that when a neutral molecule enters the focus of a time-varying electric field a dipole force is acting on the center of mass motion of the particle. The same effect is used for optical tweezing of micro-meter sized particles and biological cells. The dipole potential U is related to the dynamic (frequency dependent) polarizability of the molecule, α, and the space and time dependent distribution of the intensity of a light field E^2: $U(x,y,z,t) = -\frac{1}{4}\alpha E^2(x,y,z,t)$.

The dipole force, $F = -\nabla U$, is proportional to the gradient of the laser intensity. Assuming a Gaussian laser profile, the velocity change of the molecules in the y-direction (see Fig. 2) is obtained by integrating the force over light-matter interaction time, $\Delta v_y = \frac{1}{m}\int_{-\infty}^{\infty} F_y(t)\,\mathrm{d}t$, yielding:

$$\Delta v_y = -4y\sqrt{\frac{\pi}{2}}\frac{U}{m v_x w_0}\frac{1}{\sqrt{1+2\ln 2\left(\frac{w_0}{v_x\tau}\right)^2}}\exp\left(\frac{-2y^2}{{w_0}^2}\right), \tag{1}$$

where $x = v_x t$ describes the longitudinal motion of the molecule and τ is the light-molecule interaction time. Earlier experiments using dipole force observed the change in velocity for a pulsed beam of small molecules interacting with an individual tightly focused laser pulse of diameter 10 μm [4]. In contrast we will measure the transverse effect by its net increase in molecular beam flux at a certain spatial area at the detector.

First, we model the dipole force effect on the motion of neutral molecules for a quasi-continuous laser beam of increasing the laser waist w_0 where a test particle is propagating through the potential energy landscape of focused light (Eqn. 1). The calculated total change in transverse velocity (Δv_t) for a molecule passing through the laser spot of different waist is shown in Fig. 1a). A single dispersion profile for w_0=154 μm is shown in Fig. 1b). As expected, increasing the beam waist at a given laser power leads to a reduction in the transverse velocity effect. second, from trajectory simulation by randomly sampling of starting conditions for position and transverse velocity (Monte Carlo) we model the effect of multiple pulses acting on individual molecule trajectories. Molecule distributions simulated with and without laser interactions are shown in Fig. 2 b) indicating a clear squeezing of the spatial molecule distribution in y-direction for the case with laser 'on'.

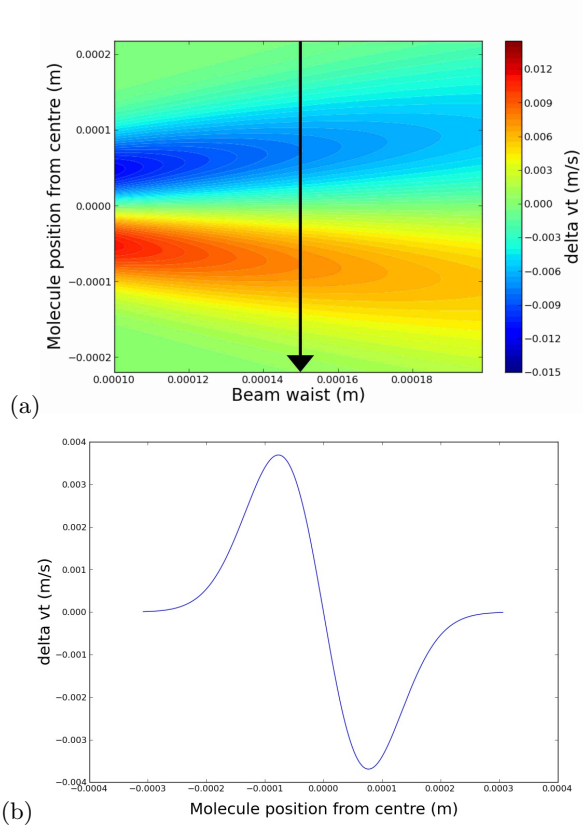

FIG. 1. (a) Model showing the total change in velocity of a test molecule (C_{60}) traveling with initially zero transverse velocity (perfect collimation) through a focused laser for different beam waists and positions along the Gaussian profile of the laser. (b) total velocity change for a beam waist of 154 μm, cut through (a) along arrow. In both simulations the following parameters were used m_{C60}=720 amu, v_x=180 m/s, pulse length=100 fs, α_{C60}=90 $\mathring{A}^3$, r=76 MHz, P_{peak}=60 kW.

Experiments have been performed with C_{60} fullerene beams formed by sublimation in an oven (Sigma Aldrich, 99.9% purity). The longitudinal velocity v_x was selected

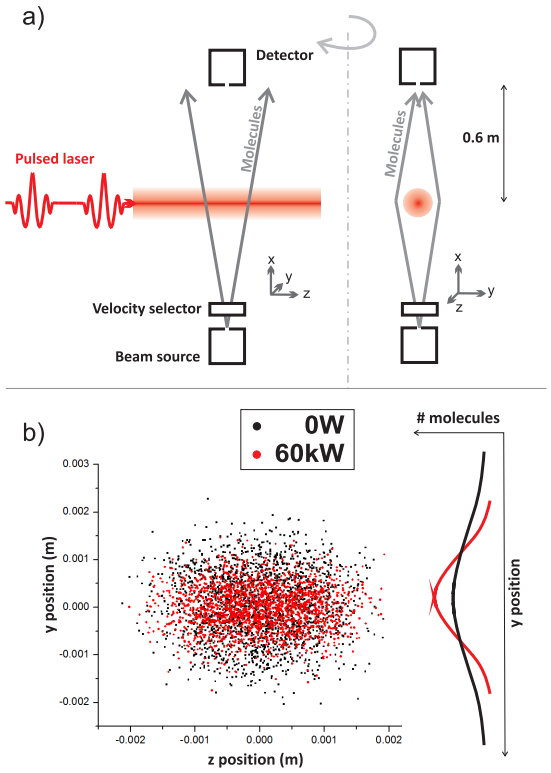

FIG. 2. (a) Schematics of the experimental setup and the geometry of the focusing effect. This affects only one spatial direction of the molecule beam due to the light intensity gradient - an elliptic lens. Light focusing in z-direction is too weak to have an effect. (b) Molecule as counted in the detector plane by Monte Carlo trajectory simulations showing the qualitative effect of the lensing with laser (red points) compared to detected molecules without laser (black points) for the same parameter as for the simulations of the dipole potential in Fig. 1. The energy is per laser pulse.

to be 180 m/s with a longitudinal spread of $\Delta v/v = \pm 2.2\%$ (FWHM) [6]. The molecular beam is collimated by a 1 mm aperture (collimation is about 1 mrad) before it is crossed with a pulsed laser (Coherent MIRA, pulse duration 100 fs, peak power 10 nJ, wavelength 800 nm) aligned along the z-axis. The laser beam was focused by a f = 100 cm lens to have a waist of about 100 μm at the light-molecule crossing. The vacuum chamber was kept at a pressure of 1×10^{-8} mbar. See for setup Fig. 2a). Molecules are detected by a Quadrupole Mass Spectrometer (Extrel) aligned in the x-axis, at a distance of 0.6 m after the light-molecule crossing. Spatial cross sections of the molecular beam were detected by moving the detector position with respect to the molecule beam or using sub-mm apertures and slits aligned in the z- and y-axis in front of the detector.

On-Off switching effect: Fig.3(a) shows experimental data of a series of nine consecutive measurements with the laser on or off. The average 'laser-on' power was 350 mW. Every data point represents the average of molecule counts over 13 minutes. We used a 0.5 mm pinhole in front of detector to measure only the center region of the molecular beam, where we expect an increase of detected molecules. We observe a clear modulation of the number of molecules being detected. Error bars are the standard deviation. Fluctuations of the detected signal are caused by molecular beam flux variations, laser instabilities as well as fluctuations in the QMS detector. The laser intensity was checked to be sufficiently stable for the time of the measurement. Integration time was chosen to reduce long term fluctuations while allowing for optimal signal to noise ratio from averaging. The experiment has been repeated several times with apertures of different size and shape in front of the detector and with a different molecule: tetra-phenyl porphyrin (TPP, 614 amu). All measurements support our observation of a transverse modulation of molecular motion. Although we observe only a small effect, this is the first experimental evidence for an optical dipole force effect on the center of mass motion of large molecules resulting from interactions with multiple light pulses. The spatial resolution of a scanning aperture method was not sufficient to image a focusing effect in the total beam profile.

Linear power dependency: To investigate the effect further we vary the laser power and observe the number of molecules detected. We observe a linear power dependency of the count rate in agreement with Eqn. 1 (see Fig. 3(b)). Data are an average of 52 measurement sequences taken over 15 seconds for each laser power subsequently, to reduce the effect of systematic count rate drifts. An maximal 8% increase in total count rate was observed for a maximum average laser power of 420 mW. This value is replicated with our Monte Carlo simulations which are shown by the red line in Fig. 3(b). Simulated trajectories of 10^5 molecules for different laser powers show the same linear dependency of the total molecule counts, in perfect agreement with the experiment for a laser beam waist of $w_0 = 154$ μm, which was the only free parameter in the Monte Carlo simulations. This is in agreement with the optics setup of the experiment. Each molecule interacts on average with 63 light pulses. The maximum laser intensity at the center of the beam waist is 4.4×10^8 W/cm^2.

Competing effects: Arguably, a single 800 nm photon cannot ionize C_{60}. Multiphoton ionization becomes significant for intensities of approximately $10^{13}W/cm^2$ [7]. In our experiment, the peak intensity of pulses is of the order $10^8W/cm^2$, well below the ionization threshold. It has been shown that femtosecond lasers can be used to increase ionization rates in large molecules compared to nanosecond pulses and to study the dynamics of the ionization process [8]. In our experiment the average number of absorbed photons is: $N_{abs} = \frac{2P\sigma\tau}{\pi\omega_0^2 h\nu}$, where τ is the interaction time between light of frequency ν and molecule, h is Planck's constant. We use the absorp-

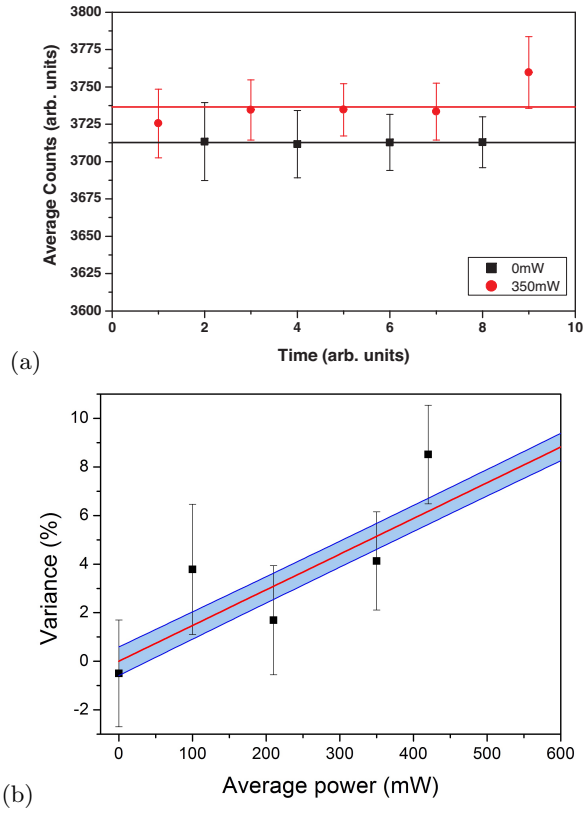

FIG. 3. Experimental results of C_{60} transverse manipulation, with standard error from 52 averaged measurement runs. (a) shows the number of molecules detected as affected by switching the laser on (350 mW average power) and off. (b) Average laser power dependence of the number of molecules detected, the red line shows the results of Monte Carlo simulations for a beam waist of 154 μm, the blue area shows the 95% confidence range.

tion cross section of $\sigma = 6{\times}10^{-20}\mathrm{cm}^{-2}$ for C_{60} at 800 nm [9] to estimate an total average value of $2.5{\times}10^{-4}$ photons absorbed by a molecule if it passes through the center of the laser. With this we can exclude all competing effects which depend on photo-absorption such as ionization, fragmentation or dissociation to explain our observation. Furthermore the significance of photon recoil effecting the center of mass motion of molecules can be neglected [10].

We now argue that this manipulation technique is universal and applicable to any polarizable particle as both mass and polarizability scale with the volume of the particle. The polarizability to mass ratio for C_{60} is given by $\alpha/\mathrm{m} = 0.1\ \mathring{A}^3/\mathrm{amu}$. This ratio typically differs only by maximally $\pm 15\%$ for other molecules and particles [11] and it is easily possible to change the optical potential U by a factor of two through modulation of laser power, which would more than compensates the α/m variation. The multiple pulse interaction may open the door to new light-molecule manipulation schemes as adding a new degree of freedom for handling.

In summary, we have observed a clear effect of multiple light pulses on the center of mass motion of neutral molecules. Further experiments are needed to optimize the light-molecule interaction effect. Simulations predict large deflection for high laser pulse energy as from ns-pulsed lasers, which have lower laser pulse repetition rates. Generally, the experiment can also be performed with high intensity continuous lasers. However more damage to the molecule is expected.

Acknowledgement: We thank the UK STFC laser loan pool for lending the laser, the UK South-East Physics Network (SEPnet) for a scholarship (P V), as well as the Foundational Questions Institute (FQXi) and the John F Templeton foundation for generous support.

* h.ulbricht@soton.ac.uk

[1] T. Seideman, J Chem Phys **106**, 2881 (1996).
[2] H. Stapelfeldt and et.al, Phys. Rev. Lett. **79**, 2787 (1997).
[3] H. Sakai and et al., Phys. Rev. A **57**, 2794 (1998).
[4] B. Zhao and et al., Phys. Rev. Lett. **85**, 2705 (2000).
[5] R. Fulton and et al., Phys. Rev. Lett. **93**, 243004 (2004).
[6] C. Szewc and et al., Rev. Sci. Instr. **81**, 81 (2010).
[7] S. Hunsche and et al., Phys. Rev. Lett. **77**, 1966 (1996).
[8] R. Weinkauf and et al., J. Phys. Chem. **98**, 8381 (1994).
[9] N. Gotsche and et al., Laser Physics **17**, 1 (2007).
[10] S. Nimmrichter, K. Hornberger, H. Ulbricht, and M. Arndt, Phys. Rev. A **78**, 063607 (2008).
[11] K. D. Bonin and V. V. Kresin, *Electric-Dipole Polarizabilities Of Atoms, Molecules, And Clusters* (World Scientific Publishing Singapore, 1997).